INTERNATIONAL JOURNAL OF REMOTE SENSING, 2017
https://doi.org/10.1080/01431161.2017.1399479

Taylor & Francis
Taylor & Francis Group

Increased chlorophyll-*a* concentration in the South China Sea caused by occasional sea surface temperature fronts at peripheries of eddies

HaiJun Ye[a], Muhsan Ali Kalhoro[a,b], Evgeny Morozov[a], DanLing Tang[a], SuFen Wang[a] and Philipp R. Thies[c]

[a]State Key Laboratory of Tropical Oceanography, Guangdong Key Laboratory of Ocean Remote Sensing, South China Sea Institute of Oceanology, Chinese Academy of Sciences, Guangzhou, China; [b]Faculty of Marine Sciences, Lasbela University of Agriculture, Water and Marine Sciences, Uthal, Pakistan; [c]College of Engineering, Mathematics and Physical Science, Renewable Energy Research Group, University of Exeter, Penryn, UK

ABSTRACT

This study investigates the processes of occasional sea surface temperature (SST) fronts and their impacts on chlorophyll-*a* concentration (chl-*a*) in the South China Sea (SCS), based on satellite remote sensing and *in situ* observations in 2009–2013. The SST fronts were detected by an entropy-based edge detection algorithm method from satellite-derived SST images with a 0.011° grid size. Three offshore SST front case studies (S1, S2 and S3) at the peripheries of eddies in the northern SCS were studied. In case S1 in September 2013, two SST fronts were detected with gradient magnitudes (GMs) greater than 0.06°C km^{-1} in the cyclonic eddy and 0.08°C km^{-1} in the periphery waters, and the fronts only existed for one and two days, respectively. After three and seven days, the high chl-*a* was found in the strong SST front waters which were about 51 and 54% higher than the concentration in the surrounding waters. The depth of the maximum chl-*a* elevated from the subsurface (50 m) to the surface. In case S2 in August 2013, two SST fronts were detected at the periphery of an anti-cyclonic eddy with GM stronger than 0.06°C km^{-1} and only existed for one day. After two days, the chl-*a* in the SST front waters was about 40% higher than the levels in the surrounding waters. In case S3 in June 2009, the GM of the eddy-feature SST front was stronger than 0.12°C km^{-1} and existed for three days, which was generated by tropical cyclone Linfa. The chl-*a* in the eddy-feature phytoplankton bloom was 6 times higher than in the surrounding waters. The results show that, in general, occasional offshore SST fronts at peripheries of eddies have stronger influence on surface chl-*a*, comparing to those seasonal coastal and permanent offshore SST fronts, via 'Wind Pump' effects.

ARTICLE HISTORY
Received 5 February 2017
Accepted 23 October 2017

1. Introduction

The sea surface temperature (SST) front is an important feature in oceanography and marine ecology. Ocean fronts are typical mesoscale oceanic phenomena identified by a

CONTACT Danling Tang lingzistdl@126.com South China Sea Institute of Oceanography, Chinese Academy of Sciences, 164 West Xingang Road, Haizhu District, Guangzhou 510301, P.R. China

discontinuity in temperature, salinity or nutrient and chlorophyll-*a* content (Belkin, Cornillon, and Sherman 2009). Chlorophyll-*a* concentration (chl-*a*) and SST govern the ocean primary productivity. Their variations may be caused by the water currents, eddies and fronts (Tang, Kawamura, and Luis 2002). The above factors are related to phytoplankton biomass which is the basic component in marine food chains (Dwivedi et al. 2005). Variability of fronts leads to an enhanced exchange of phytoplankton and chemical properties across the front which affects the local phytoplankton diversity and biomass (Clayton et al. 2013).

According to previous studies, the oceanic fronts were classified according to their position providing a distinction between: coastal fronts, shelf fronts and offshore water fronts (Yanagi and Koike 1987). Regarding timescales, we classify the oceanic fronts to permanent, seasonal and occasional fronts, while occasional fronts exist less than 10 days. Front structures are also important for the biophysical interactions across the coastal regions (Stegmann and Ullman 2004). A considerable number of studies on the relationship between fronts and chl-*a* have been conducted on the permanent and seasonal fronts in coastal, shelf and open ocean (Tang, Kawamura, and Luis 2002; Rivas 2006; Taylor et al. 2012; Clayton et al. 2013). However, studies of occasional offshore front's effects on chl-*a* have been rarely reported.

The South China Sea (SCS) is a large and semi-enclosed marginal ocean basin, with a total area of 3.5 million km^2 and an average depth of 1212 m. It is bordered by the East China Sea on the north-east, the Pacific Ocean and Sulu Sea on the east, and the Java Sea and the Indian Ocean on the south-west. The spatial and temporal distribution of the seasonal and permanent SST fronts, and its genesis and impact on chl-*a* in the SCS have been widely studied (Wang et al. 2001; Belkin and Cornillon 2003; Lan et al. 2009; Chang et al. 2010; Liu et al. 2010; Wang et al. 2012; Yao et al. 2012; Jing et al. 2016). Tang, Kawamura, and Luis (2002) reported short-time variations of chl-*a* in the eddy, using Sea-viewing Wide Field-of-view Sensor and SST data. The northern SCS is also a region of high probabilities of eddy occurrence (Chen et al. 2007; He, Zhan, et al. 2016). Eddy pumping generates upwelling in a cyclonic eddy and downwelling in an anti-cyclonic eddy which can result in enhanced and depressed chl-*a* within cyclonic eddy and anti-cyclonic eddies, respectively (Mizobata et al. 2002; Chelton et al. 2011). The chl-*a* is also enhanced at the periphery of anti-cyclonic eddies (Mizobata et al. 2002).

Remote sensing studies on SST fronts were conducted at different areas, such as the Arabian Sea (Vipin et al. 2015), the western South Atlantic (Saraceno, Provost, and Piola 2005), the Kuroshio Extension (Clayton, Nagai, and Follows 2014), California current ecosystem (Kahru et al. 2012; Taylor et al. 2012), Taiwan Bank in the SCS (Lan et al. 2009) and Luzon Strait (Qiu et al. 2012), it was found that they can change phytoplankton community structures (Taylor et al. 2012). This biogeochemical signature of SST fronts has positive effects on the fish population, and thus, frontal regions are often being exploited for commercial fishing (Alemany, Acha, and Iribarne 2014; Tseng et al. 2014). Those studies proved that SST gradients can enhance chl-*a* in the waters.

Due to dynamic ocean properties, SST is one of the most important parameters of oceanographics from physical and biological perspectives, but it is difficult to make *in situ* observations. Satellite remote sensing has enabled global monitoring of oceanic SST gradients from space, and it is also the most effective method to monitor the

environmental changes in the SCS. The reliable SST fronts data of high spatial and temporal resolution can be used to investigate the positions and intensity of fronts.

Previous studies on SST fronts were based on seasonal variation and performed with the use of *in situ* data, which were mainly focused on the coastal areas using different analyses methods. The present study focuses on the generation of occasional offshore SST gradients and their impact on chl-*a*, and the study is based on *in situ* and satellite data in the SCS.

2. Materials and methods

2.1. *Selection criteria for three occasional fronts*

Three occasional offshore fronts at the peripheries of eddies between 2009 and 2013 were analysed, considering data availability, high intensity of events and representation of different hydrodynamic conditions. Case 1 was located at the periphery of a cyclonic eddy on 18–24 September 2013, where high chl-*a* maximum on surface was captured by a research cruise conducted in September 2013. Case S2 was located at the periphery of an anti-cyclonic eddy during 23–26 August 2013 that was one of the strongest anti-cyclonic eddies in the SCS in the study period of 2009–2013. Case S3 was located at the periphery of a cyclonic and an anti-cyclonic eddy during 22–24 June 2009 after the passage of typhoon Linfa in 2009, while we observed a very strong chl-*a* concentration around case S3 front.

2.2. *Satellite products*

The Aqua Moderate Resolution Imaging Spectroradiometer (MODIS) and Visible Infrared Imaging Radiometer Suite (VIIRS)-derived sea surface phytoplankton chl-*a* product with 1 km spatial resolution was obtained from National Aeronautics and Space Administration (NASA) OceanColor (http://oceancolor.gsfc.nasa.gov). The daily multiscale ultrahigh resolution (MUR) SST analysis data set with a spatial resolution of 0.011° produced by merging data from MODIS, Advanced Microwave Scanning Radiometer-Earth Observing System and Advanced Very High Resolution Radiometer is available from June of 2002 and can be obtained from the NASA Jet Propulsion Laboratory (http://data.nodc.noaa.gov/ghrsst/L4/GLOB/JPL/MUR/). Daily fields of absolute geostrophic currents derived from merged altimeter products and merged Sea Level Anomaly (SLA) were obtained from the website for the Archiving, Validation and Interpretation of Satellite Oceanographic data at www.aviso.oceanobs.com. The daily remote sensing fields of sea surface winds (at 10 m above the sea surface) with a 0.25° × 0.25° resolution were obtained from the Advanced Scatterometer website at ftp.ifremer.fr/ifremer/cersat/products/. The track data for typhoon Linfa (2009) were taken from the Joint Typhoon Warning Center http://weather.unisys.com/hurricane/ and https://en.wikipedia.org/wiki/Tropical_Storm_Linfa_(2009).

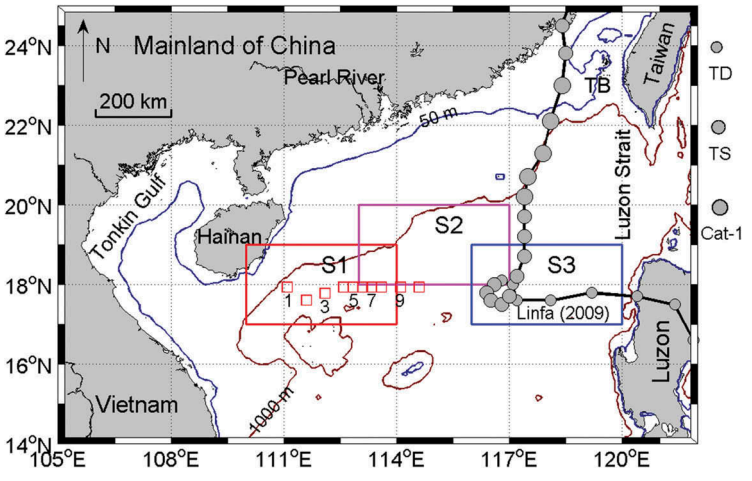

Figure 1. Geographical location of the South China Sea, showing three case study regions S1, S2 and S3. The red squares (S1) denote the cruise CTD stations from which stations 1–7 were conducted on 26 September 2013 while stations 8–10 were conducted on 1 October 2013. TB denotes Taiwan Bank. The 6 hourly positions of typhoon centres are marked by dots, of which sizes represent the intensity of typhoon Linfa (June 2009). Abbreviations are used for tropical depression (TD), tropical storm (TS) and Category-one typhoon (Cat-1).

2.3. *In situ observations*

The shipboard temperature and salinity were determined with a Seabird SBE CTD profiler. As shown in Figure 1, a total of 10 stations were conducted from which stations 1–7 were conducted on 25–26 September 2013 and stations 8–10 were conducted on 1 October 2013 during research cruise organized by the South China Sea Institute of Oceanography, Chinese Academy of Science. Water samples for chl-*a* and nutrients analysis were taken at 0, 25, 50, 75, 100, 150 and 200 m water depth. Nutrients water samples were pre-filtrated through a Whatman GF/F filter, and concentrations of nitrate (NO_3^-) were analysed by standard spectrophotometric methods. The detection limits of nitrate were 0.003 mg l^{-1}. Sea water samples for chl-*a* were determined by filtering 500–1000 ml sea water through a Whatman GF/F glass fibre filter. The filter papers were stored at –20°C and extracted in 90% acetone, and fluorescence was measured following Parsons, Maita, and Lalli (1984) using a Turner Design 10 fluorimeter.

2.4. *Calculation of SST gradient magnitude*

A gradient-based method is commonly used to recognize and determine the ocean fronts (Belkin and O'Reilly 2009; Lan et al. 2009; Huang, Zhang, and Zhou 2010; He, Huang, and Zeng 2016). The intensity of the SST front is quantitatively estimated by the SST gradient magnitude (GM) in each geo-referenced grid. The SST GM at a given pixel was defined as follows:

$$\mathrm{GM} = \sqrt{(\partial T/\partial x)^2 + (\partial T/\partial y)^2}\ (^{\circ}\mathrm{Ckm}^{-1}), \tag{1}$$

where T is SST, and the x and y axes are, respectively, directed towards the east and north. The GM was computed at all pixels for each image. Note that, since the MUR SST data have a spatial resolution of 0.011° × 0.011° (≈ 1.2 km × 1.2 km), the SST GM was divided by 1.2 in the upper equation. The gradient threshold was set at 0.06°C km^{-1} (Saraceno, Provost, and Piola 2005), and only the regions with GM greater than the threshold can be defined as front.

3. Results

3.1. *Case S1 on 21–24 September 2013*

A weak cyclonic eddy (negative SLA, bold contours) centred at 18.2°N, 111.7°E and a strong anti-cyclonic eddy (positive SLA, bold contours) were observed during the case S1 (Figure 2 (a)). On 20 September 2013, low SST patch of about 27.5°C occurred in the cyclonic eddy (Figure 2a(iii)) and then it became cooler on 21 September 2013 (Figure 2a (iv)). It became warmer and moved north-eastward to the periphery of the weak cyclonic eddy during the following 3 days. It should be noted that the low-temperature patches were also found in the coastal area during 19–22 September 2013 (Figure 2a(ii-x)). The SST patch higher than 29°C occurred in the anti-cyclonic eddy.

The SST gradient distribution shown in Figure 2(b) indicates three strong SST fronts. During 19–21 September 2013, a very strong coastal SST front with GM higher than 0.08° C km^{-1} occurred in east coastal areas of Hainan Island (Figure 2b(iii–iv)) and it weakened in the following 3 days (Figure 2b(v-vii)). However, the first offshore SST front with GM > 0.08°C km^{-1} occurred at 17.3°N, 112°E at the periphery of the weak cyclonic eddy on 18 September 2013 (Figure 2b(i)) and it weakened to 0.06°C km^{-1} on 19 September 2013 (red arrows) (Figure 2b(ii)). The geostrophic currents were at about 0.2 m s^{-1} and moved north-eastward. The second offshore SST front started on 20 September 2013 (GM about 0.05°C km^{-1}) and strengthened (GM > 0.06°C km^{-1}) on 21 September 2013 at 18°N, 112° E at the centre of the weak cyclonic eddy (blue arrows) (Figure 2b(iii–iv)). It rotated around the cyclonic eddy where the geostrophic current was less than 0.1 m s^{-1}. It was observed that both offshore SST fronts were surrounded by higher temperature waters.

The VIIRS chl-*a* image on 24 September 2013 overlaid over the SST GM map on 21 September 2013 showed that the high chl-*a* patch occurred around the high SST gradients at 18°N, 112°E (Figure 2c(vii)). The high chl-*a* patch of about 0.166 mg m^{-3} was observed in the cyclonic eddy which is about 51% higher than in the surrounding waters (0.111 mg m^{-3}). This high chl-*a* patch was matched well with the second offshore SST front. Unfortunately due to cloud coverage, no data could be obtained to derive chl-*a* images on 18–23 September 2013 (Figure 2c(i-vi)).

The above analyses were generally focused on oceanographic conditions at the sea surface. Figure 3 represents vertical profiles of temperature, salinity and chl-*a*, based on *in situ* observations from stations 1–7 which were conducted on 26 September 2013 and stations 8–10 were conducted on 1 October 2013 (indicated by numbers in Figure 1). The water masses with relatively low temperature (< 28.8°C) were observed at stations 3–4, while the water masses with relatively high temperature (> 29°C) were observed in other stations (Figure 3(a)). The combination of low temperature in the upper layer and shallow mixed layer depth at stations 3–4 is an indication of relatively strong upwelling,

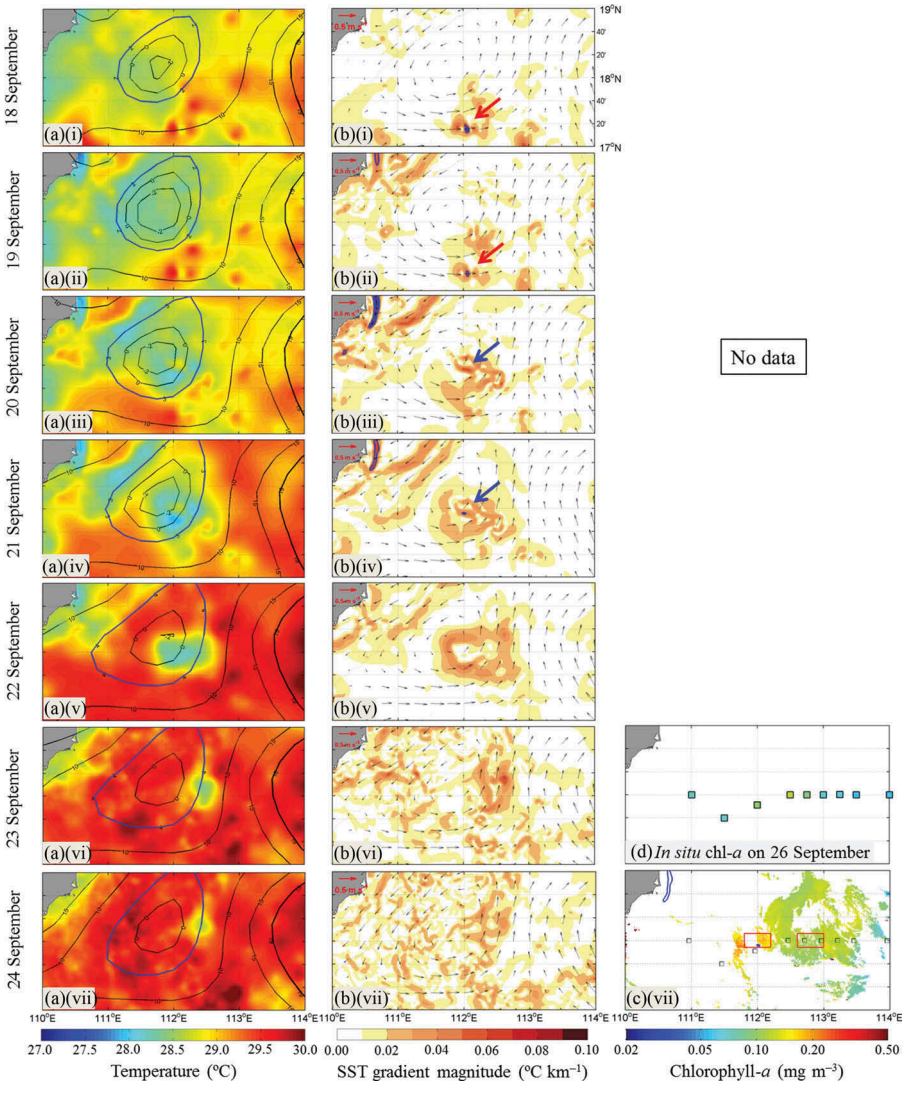

Figure 2. Satellite images of the case S1 (a) sea surface temperature (SST) overlaid onto Sea Level Anomaly (SLA), bold black/blue contour lines show anti-cyclonic/cyclonic eddies, (b) SST gradient magnitude(GM) overlaid onto geostrophic currents, blue contours represent GM greater than 0.06°C km^{-1}; red/blue arrows show first/second offshore SST front, (c) chlorophyll-*a* (chl-*a*) overlaid onto SST fronts (blue contour lines) on 21 September 2013, black squares indicating *in situ* observations, two red boxes show higher chl-*a* (0.166 mg m^{-3}) concentration in the SST front waters compared to the surrounding waters (0.111 mg m^{-3}) during 24 September 2013 and (d) *in situ* chl-*a* observed on 26th September during 2013 in the SCS.

a common phenomenon in cyclonic eddies. The low salinity at the station 3 was due to the large rainfall (Ye et al. 2017). A unique high salinity patch (>34 psu) was observed between 40 and 50 m at stations 5–6, which indicates that the deep waters had upwelled to the base of mixed layer (Figure 3(b)). The relatively low temperature and high salinity were observed at stations 8–10 on 1 October 2013 which were affected by typhoon Wutip (Ye et al. 2017).

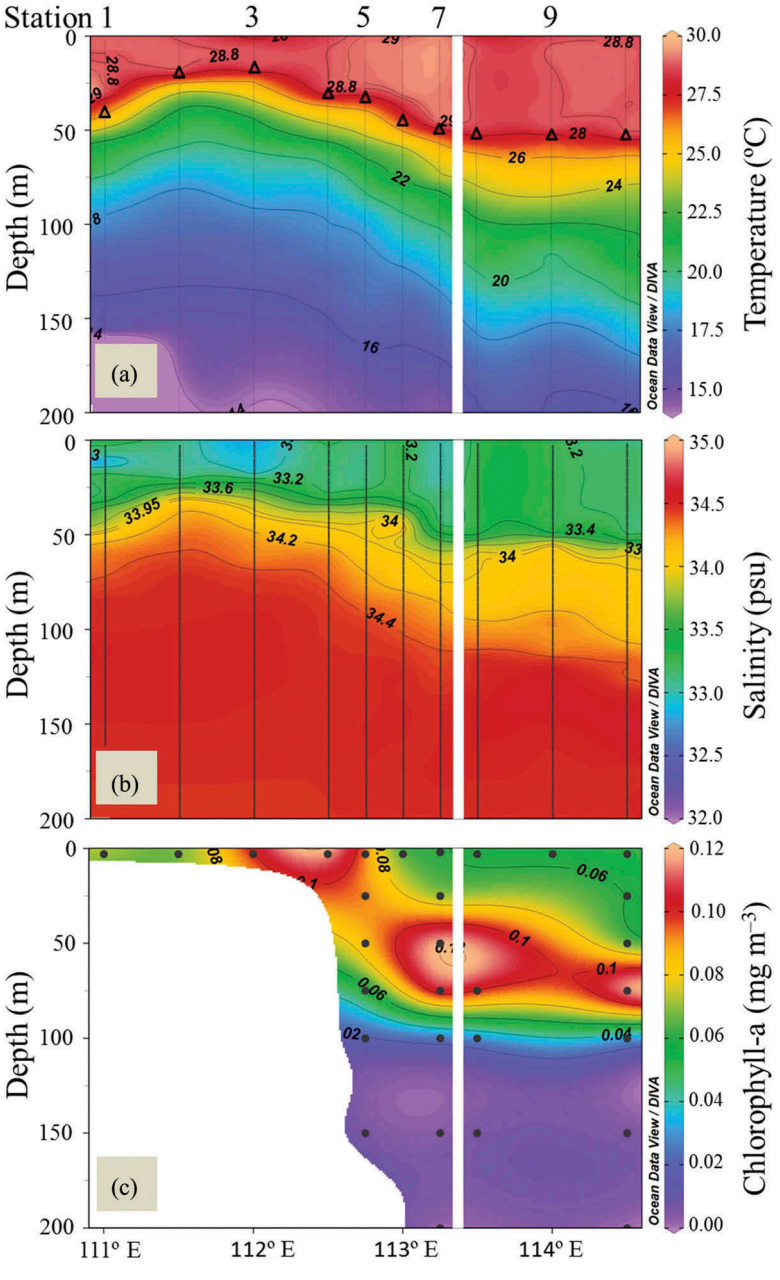

Figure 3. *In situ* vertical profiles of (a) temperature (°C), (b) salinity (psu) and (c) chl-*a* concentration (mg m^{-3}) at different depth intervals from stations 1 to 7 on 26 September 2013 and stations 8 to 10 on 1 October 2013 in the South China Sea. The triangles represent the mixed layer depth.

The *in situ* chl-*a* data were also sampled in the case S1 study region. The high surface chl-*a* patch (mean value = 0.103 mg m^{-3}) at stations 3–5 centred at 18°N, 112.5°E at the periphery of the weak cyclonic eddy and high subsurface chl-*a* patch (> 0.1 mg m^{-3}) at stations 7–10 from 113.25°E to 114.5°E across the periphery of the strong anti-cyclonic eddy were observed (Figures 2(d) and 3(*b*)). Subsurface chl-*a* maximum occurred at

50–75 m depth from stations 7 to 10, which is a common phenomenon in the open ocean. The maximum chl-*a* at station 5 that occurred at the surface is unusual, and it may be due to the strong occasional SST gradients on 20–21 September 2013 which uplifted the subsurface nutrient and chl-*a* rich water to the surface.

3.2. *Case S2 on 24–26 August 2013*

The SST gradient formation was observed during 24–26 August 2013. Figure 4 illustrates the distribution of SST, SST gradients and chl-*a* from satellite observations in the case S2 region. It was observed that the high SST patch of about 29.5°C was found on the periphery of an anti-cyclonic eddy (bold black contours) on 23–26 August 2013 (Figure 4 (a)). However, on 23 August 2013, the low SST patch of about 28.5°C appeared on the left side of the anti-cyclonic eddy and then it became warmer during the following 3 days. A strong SST front (GM > 0.06°C km^{-1}) occurred at the boundary between cold and warm SST patches at 18.7°N, 114.5°E on 24 August 2013 (Figure 4b(ii)) and weakened to less than 0.06°C km^{-1} on 25–26 August 2013 (Figure 4b(iii–iv)). Another SST front (GM > 0.06°C km^{-1}) surrounded by high temperature was observed at 118°E, 19.3°N on 25 August 2013 (Figure 4b(iii)) and then weakened on 26 August 2013 (Figure 4b(iv)).

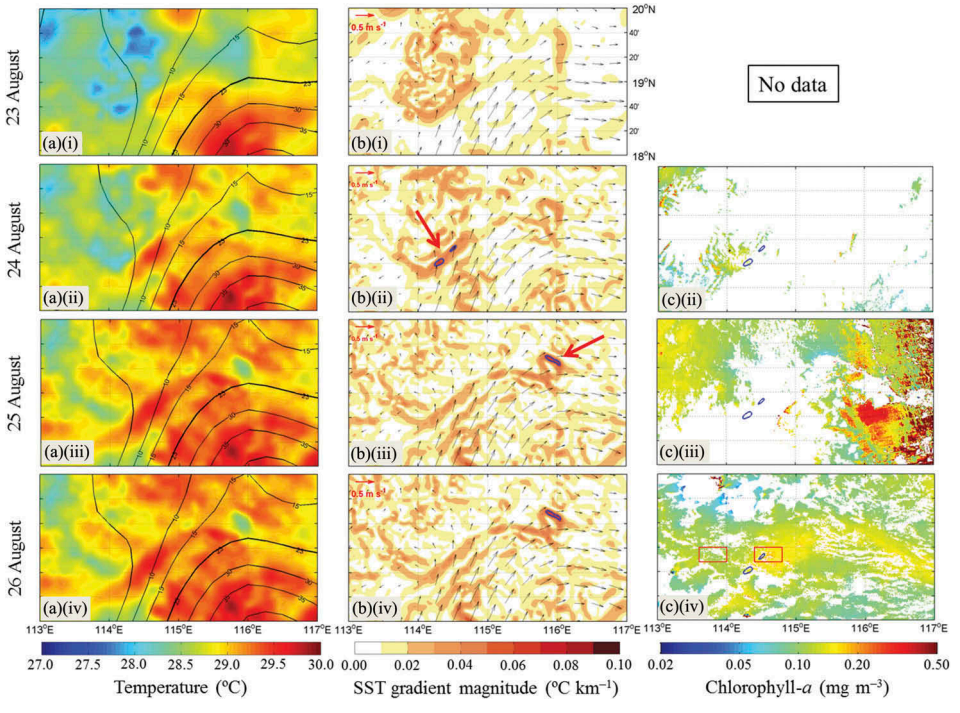

Figure 4. Satellite images of case S2 (a) SST overlaid onto SLA, bold black contour lines show anticyclone eddies, (b) SST GM overlaid onto geostrophic currents, blue contour lines show strong SST GM (>0.06°C km^{-1}), (c) VIIRS-derived chl-*a* images overlaid over SST fronts (blue contour lines) on 24 August 2013, red boxes show higher chl-*a* (0.154 mg m^{-3}) in the SST front waters compared to the surrounding waters (0.110 mg m^{-3}) on 26 August 2013 in the SCS.

The maximum geostrophic currents about 0.6 m s^{-1} occurred at the periphery of the anti-cyclonic eddy.

The VIIRS chl-*a* images on 24–26 August 2013 overlaid over the SST gradients map on 24 August 2013 showed that a high chl-*a* patch occurred at the periphery of the anti-cyclonic eddy (Figure 4c(ii)). It was observed that this high chl-*a* patch moved with the geostrophic currents. Two days after the generation of the SST front, average chl-*a* in the red box (Figure 4c(iv)) was 0.154 mg m^{-3} which is 40% higher than the levels in the surrounding waters 0.110 mg m^{-3}. Abnormally high chl-*a* values on 25 August 2013 could possibly be caused by satellite algorithm overestimation of chl-*a* due to cloud-induced features and/or subsequent errors in the atmospheric correction (Figure 4c(iii)).

3.3. *Case S3 on 22–25 June 2009*

The study region of case S3 was located in the deep water area of the north-east SCS. Positive SLA combined with clockwise geostrophic currents indicates an anti-cyclonic eddy (bold black contours) at 17°N, 118°E. The small positive SLA combined with anticlockwise geostrophic currents indicates the presence of a weak cyclonic eddy (bold blue contours) at 18.2°N, 117.8°E on 22–25 June 2009 (Figure 5(a)). The low SST patch of about 27°C occurred in the weak cyclonic eddy, and it became slightly warmer in the next three days. The SST in the anti-cyclonic eddy is higher than in the cyclonic case. An eddy-feature front was observed on 22–24 June 2009 (Figure 5b(i–iii)). In the south of the eddy-feature front (black arrows), a strong SST GM greater than 0.1°C km^{-1} formed at the periphery of the weak cyclonic and anti-cyclonic eddies on 22 June 2009 (Figure 5b(i)), strengthened up to 0.12°C km^{-1} on 23 June 2009 (Figure 5b(ii)) and then it begun weakening to less than 0.06°C km^{-1} on 25 June 2009 (Figure 5b(iv)). Another slightly weaker SST front with GM about 0.08°C km^{-1} at the periphery of the cyclonic eddy on 23–24 June 2009 appeared in the north of the eddy-feature front (blue arrows). The green arrows in Figure 5b(i–iii)) indicate the arm of the eddy-feature front.

The MODIS Aqua chl-*a* images overlaid over SST gradients map for 22 June 2009 indicate that the high chl-*a* occurred in the cold side of the SST gradients and it was well matched with the cyclonic eddy, although the satellite image did not cover all the area because of clouds (Figure 5c(i)). On 23–25 June 2009, the high chl-*a* patch showed an eddy-feature phytoplankton bloom which was very well matched with the eddy-feature front. The strong SST gradients can be used as a boundary between high chl-*a* water and normal chl-*a* water. The high chl-*a* of 0.692 mg m^{-3} observed at the eddy-feature front waters was higher by a factor of 6, compared to the concentration of 0.098 mg m^{-3} in the surrounding normal waters (Figure 5c(iii), black boxes on 24 June 2009).

4. Discussion

4.1. *The possible mechanism of the occasional front genesis*

Numerous studies were conducted on several strong and permanent SST fronts (GM > 0.15°C km^{-1}) in the northern SCS, namely coastal fronts along the mainland China Coast, Pearl River Estuary Coast, Taiwan Banks, Hainan Island East Coast and Tonkin Gulf Coast, and slightly weaker seasonal offshore West Luzon fronts (GM < 0.08°C km^{-1}), (Wang et al.

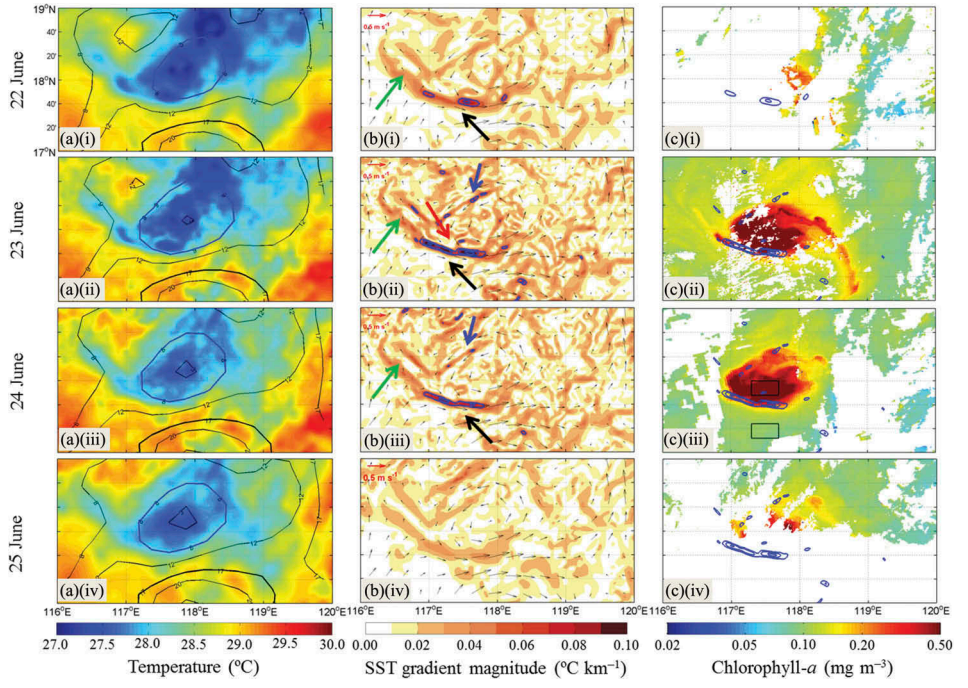

Figure 5. Satellite images of case S3 (a) SST overlaid onto SLA, bold black/blue contours lines show anti-cyclonic/cyclonic eddies, (b) SST GM overlaid onto geostrophic currents, blue contour lines show strong SST GM (>0.06°C km^{-1}) and green arrows show one arm of the eddy-feature front, (c) Aqua MODIS derived chl-*a* images overlaid onto SST fronts on 22 June 2009 and 23 June 2009 (blue contour lines), black boxes show higher chl-*a* concentration (0.692 mg m^{-3}) in the eddy-feature SST front waters compared to the surrounding waters (0.098 mg m^{-3}) on 24th June 2009 in the SCS.

2001; Chang et al. 2006, 2010; Lan et al. 2009; Zeng et al. 2014; Jing et al. 2016). Although the position and intensity of these fronts changed over time due to complex shelf dynamic processes, the fronts tend to be approximately aligned with the shelf topography throughout the year. Most of the fronts were found on the boundary of cold and warm waters which existed for a long time.

The south-westward wind on 16–17 September 2013 and strong westward wind on 18–19 September 2013 (Figure 6a(i–iv)) prevailed in the eastern Hainan Island and subsequently induced the Hainan Island East Coastal fronts on 19–21 September 2013 (Figure 2b(ii–iv)). The winds weakened on 20 September 2013 and changed to eastward on 21–22 September 2013 (Figure 6a(v-vii)), which resulted in the disappearance of the Hainan Island East Coastal fronts on 22 September 2013 (Figure 2b(v)). This observation is in agreement with previous studies that showed how the coastal upwelling mechanisms are affected by wind direction and variable topography (Jing et al. 2009; Su and Pohlmann 2009).

The present study is focused on generation of occasional offshore SST fronts in three case study regions in the northern SCS. Two offshore SST fronts were detected in the case S1, the GMs were stronger than 0.06°C km^{-1} for the front inside the cyclonic eddy and 0.08°C km^{-1} for the levels in the normal waters, and the fronts existed only for one and two days, respectively (Figure 2b(i–iv)). The SST gradient and fronts are highly

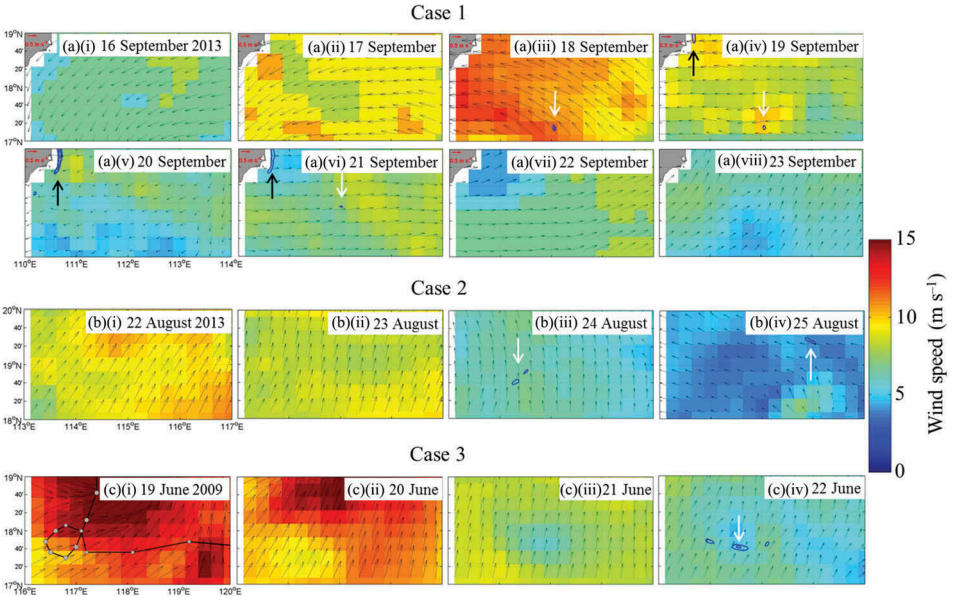

Figure 6. Satellite derived sea surface wind images overlaid into SST GM (a) case S1 during 16–23 September 2013, (b) case S2 during 22–25 August 2013, (c) case S3 during 19–22 June 2009 in the SCS, black/white arrows show coast/offshore SST front. Blue contour lines show strong SST GM (>0.06°C km^{-1}). Dots and black line represent the track of typhoon Linfa (June 2009).

influenced by the monsoon seasons (Jing et al. 2009; Su and Pohlmann 2009), we observed that, at 17.2°N,112°E, the south-westward wind on 16 September 2013 changed to slightly stronger westward wind on 17 September 2013, and it developed to strong north-westward wind on 18 September 2013 (Figure 6a(i–iii)). The sudden changes of wind intensity combined with the reversed eastward geostrophic currents might be the reason of the first offshore SST fronts generation on 18–19 September 2013 in the case S1 (Figure 2b(i–ii)). Also in the second offshore SST front region, the strong westward wind on 17–19 September 2013 (Figure 6a(ii–iv)) changed to slightly weaker eastward wind on 21–22 September 2013 (Figure 6a(vi-vii)). This quick reversal of wind direction may be the reason of the second offshore SST fronts generation on 21 September 2013 (Figure 2b(iv)).

The two SST fronts with GM stronger than 0.06°C km^{-1} along the periphery of an anticyclonic eddy were observed in the case S2 and both existed only for one day (Figure 4). The strong north-eastward wind on 22 August 2013 changed to slightly strong northward wind on 23–24 August 2013, and it changed to a very weak westward wind on 25 August 2013 in the case S2 (Figure 6(b)). The drastic change in wind intensity and direction coupled with the opposing geostrophic currents may be the reason of SST fronts generation on 24–25 August 2013 (Figure 4b(ii–iii)).

While the SST front with GM greater than 0.12°C km^{-1} in the case S3 existed for three days (Figure 5). Furthermore, it was observed that the reversing monsoons can generate fronts (Shimada et al. 2005; Shi et al. 2015). The strong rotating wind during the tropical cyclone on 19 June 2009 (Figure 6c(i)) changed to very weak wind on 22 June 2009 (Figure 6c(iv)). By strong 'Wind Pump' effects, tropical cyclone Linfa lingering at 18°N,

117°E on 17–19 June 2009 enhanced this eddy (Chen and Tang 2012), resulting in the strong SST fronts (GM > 0.12°C km^{-1}) on 22–24 June 2009 (Figure 5b(i–iii)).

4.2. *Effects of fronts on chl-a*

Previous studies found that the SST fronts can generate coastal (Stegmann and Ullman 2004; Rivas 2006; Lan et al. 2009; Vipin et al. 2015) and offshore phytoplankton blooms (Saraceno, Provost, and Piola 2005; Mahadevan and Tandon 2006; Taylor and Ferrari 2011; Landry et al. 2012; Taylor et al. 2012). However, those studies were carried out for permanent or seasonal SST fronts. Some reports indicate that chl-*a* on the cold side of the permanent offshore or seasonal coastal fronts increased about one to three times (Rivas 2006; Landry et al. 2012). In the presented case studies S1, S2 and S3, the overall increase of chl-*a* in the stronger SST front waters was found to be 51–54%, 40% and 608%, respectively (Table 1), compared to the surrounding waters.

Ship surveys for the purpose of comparing the satellite images with the *in situ* data were not designed to cross the fronts; therefore, *in situ* data were only occasionally obtained and the observations may have missed the actual front's location. In the case S1, the high chl-*a* values at stations 3–5 at 18°N, 112.5°E captured by ship surveys (Figure 3) were well matched with the first SST front (Figure 2). Although there are scarce satellite chl-*a* images in the case S1, we got *in situ* vertical chl-*a* profiles observations along the 18°N transect. In the first SST front waters at 17.2°N, 112°E, the geostrophic current was about 0.25 m s^{-1} (from 19 September 2013 to 26 September 2013) and then the water moved about 151 km north-eastward. This means that the front waters moved to 18°N, 112.75°E. The unusual high salinity between 40 and 50 m depth at stations 5–6 (Figure 3(b)) manifests this hypothesis. The uplifted high salinity waters supplied nutrients for phytoplankton and resulted in an unusual phenomenon of maximum chl-*a* at the surface at station 5 (Figure 3(c)). The high chl-*a* patch according to the *in situ* measurements was characterized with a concentration of 0.093–0.103 mg m^{-3} (Figure 3) on 26 September 2013 and thus might have been caused by the first SST front.

The high chl-*a* patch at 18°N, 112°E was well matched with the second SST front which rotated around the geostrophic currents and appeared after three days. Eddy pumping generates upwelling in a cyclonic eddy thus resulting in decreased SST and enhanced chl-*a* within cyclonic eddy (Chen et al. 2007; Chelton et al. 2011). The weak cyclonic eddy (negative SLA, bold contours) centred at 18.2°N, 111.7°E as indicated by low temperature in the upper layer and shallow mixed layer depth at stations 3–4 (Figures 2(a) and 3(a)) which may result in the high chl-*a* patch. The low SST patch

Table 1. Statistical relationships of three sea surface temperature (SST) fronts and chlorophyll-*a* (chl-*a*) concentration levels in the South China Sea.

Study case	SST gradient magnitude (°C km^{-1})	Existence time (days)	Chl-*a* in SST front waters (mg m^{-3})	Time lag (days)	Chl-*a* in surrounding waters (mg m^{-3})	Enhanced chl-*a* (%)
S1	> 0.08	2	0.103$^{\text{in-situ}}$	7	0.067$^{\text{in-situ}}$	54
S1	> 0.06	1	0.166^{a}	3	0.111^{a}	51
S2	> 0.06	1	0.154^{a}	2	0.110^{a}	40
S3	> 0.12	3	0.692^{b}	2	0.098^{b}	608

^{a}VIIRS; ^{b}MODIS Aqua.

moved from the centre to the periphery of the weak cyclonic eddy indicated that the second SST front also contributed to the high chl-*a* patch.

In the case S2, it was observed that the high chl-*a* patch (40% higher) appeared one or two days after the SST front. The high chl-*a* patch was moving along the direction of the geostrophic currents (Figure 4). It is well known that a high chl-*a* occurred at the periphery, in particular at the south-eastern part of an anti-cyclonic eddy (Mizobata et al. 2002; Chelton et al. 2011; He, Huang, and Zeng 2016). However, the high chl-*a* patch on 26 August 2013 was suddenly occurred at the north-western part of the anti-cyclonic eddy (Figure 4(c)). It represented that the high chl-*a* patch was mainly due to the SST front two days before.

The SST fronts can induce a greater eastward drift in the typhoons motion (Yun, Chan, and Ha 2012). Typhoons can induce a cyclonic eddy (Ye et al. 2013), and a cold SST eddy can fuel a cyclonic eddy-feature chl-*a* bloom (Tang, Kawamura, and Luis 2002). Here, we found that typhoon Linfa (2009) induced a strong SST front (GM > 0.12°C km^{-1}) after 2–4 days. The shape of this SST front has an eddy-like feature which in turn induced an eddy-feature like chl-*a* bloom (Figure 5). The chl-*a* is often gradually enhanced in the cyclonic eddy (Mizobata et al. 2002; Tang, Kawamura, and Luis 2002; Chelton et al. 2011). The eddy-feature phytoplankton bloom appeared suddenly on 22 June 2009; while in this bloom, chl-*a* was higher than the other two cases (S1 and S2) because of strong eddy-feature front. It should be noted that the 608% higher chl-*a* was observed in case S3, which maybe because of the subsurface nutrients-rich water upwelled by typhoon Linfa, which in turn can trigger strong chl-*a* bloom at surface, via 'Wind Pump' effects (Chen and Tang 2012).

It is also noticed that not only SST fronts enhance the chl-*a*, but typhoons, cyclonic and anti-cyclonic eddies, biological process with other factors also affect the chl-*a* concentrations. However, satellite data alone are not fully adequate to measure SST front impact on chl-*a*. Thus, we suggest that further analysis of satellite and *in situ* data through different modelling should be carried out to improve our understanding of chl-*a* distribution in the SCS.

5. Conclusions

Using satellite remote sensing and *in situ* data, this study is the first time to testify that occasional offshore SST fronts in the northern SCS have positive effects on chl-*a*. Three occasional SST fronts existed only for 1–3 days at the peripheries of eddies were found offshore waters. The strong SST fronts with high GM greater than 0.12°C km^{-1} enriched strong chl-*a* bloom (608%), while weak SST fronts (GM > 0.06–0.08°C km^{-1}) induced weak chl-*a* bloom (40–54%) compared to the surrounding waters. The *in situ* observations showed that high SST GM values also elevate the maximum chl-*a* from the subsurface waters (50 m) to the surface. In comparison with previous studies, the present study further reveals that occasional offshore SST fronts at the peripheries of eddies have strong influence on chl-*a*, not only at the surface but also along the vertical profile, via 'Wind Pump' effects.

Acknowledgements

This study was funded by Key Project of the National Natural Sciences Foundation of China (NSFC 41430968), Group Project of High-end Foreign Experts Recruitment Program Guangdong, China (GDJ20154400004), Project of Guangdong Key Laboratory of Ocean Remote Sensing and NRSCS-EAS Dragon Program 4 (ID 10689) award to DanLing Tang. Muhsan Ali Kalhoro was supported by China Science and Technology Exchange Center, Ministry of Science and Technology for awarding Talented Young Scientist Award (PAK-16-021). The authors thank the South China Sea Research Cruise, R/V Shiyan 3 in 2013.

Disclosure statement

No potential conflict of interest was reported by the authors.

Funding

This work was supported by the Key Project of the National Natural Sciences Foundation of China [NSFC 41430968]; NRSCS-EAS Dragon Program 4 [ID 10689]; Project of Guangdong Key Laboratory of Ocean Remote Sensing; Group Project of High-end Foreign Experts Recruitment Program Guangdong, China [GDJ20154400004]; China Science and Technology Exchange Center, Ministry of Science and Technology for awarding Talented Young Scientist Award [PAK-16-021].

References

Alemany, D., E. M. Acha, and O. O. Iribarne. 2014. "Marine Fronts are Important Fishing Areas for Demersal Species at the Argentine Sea (Southwest Atlantic Ocean)." *Journal of Sea Research* 87: 56–67. doi:10.1016/j.seares.2013.12.006.

Belkin, I. M., and J. E. O'Reilly. 2009. "An Algorithm for Oceanic Front Detection in Chlorophyll and SST Satellite Imagery." *Journal of Marine Systems* 78 (3): 319–326. doi:10.1016/j.jmarsys.2008.11.018.

Belkin, I. M., and P. Cornillon. 2003. "SST Fronts of the Pacific Coastal and Marginal Seas." *Pacific Oceanography* 1 (2): 90–113.

Belkin, I. M., P. C. Cornillon, and K. Sherman. 2009. "Fronts in Large Marine Ecosystems." *Progress in Oceanography* 81 (1): 223–236. doi:10.1016/j.pocean.2009.04.015.

Chang, Y., T. Shimada, M.-A. Lee, H.-J. Lu, F. Sakaida, and H. Kawamura. 2006. "Wintertime Sea Surface Temperature Fronts in the Taiwan Strait." *Geophysical Research Letters* 33: 23. doi:10.1029/2006GL027415.

Chang, Y., W.-J. Shieh, M.-A. Lee, J.-W. Chan, K.-W. Lan, and J.-S. Weng. 2010. "Fine-Scale Sea Surface Temperature Fronts in Wintertime in the Northern South China Sea." *International Journal of Remote Sensing* 31 (17–18): 4807–4818. doi:10.1080/01431161.2010.485146.

Chelton, D. B., P. Gaube, M. G. Schlax, J. J. Early, and R. M. Samelson. 2011. "The Influence of Nonlinear Mesoscale Eddies on Near-Surface Oceanic Chlorophyll." *Science* 334 (6054): 328–332. doi:10.1126/science.1208897.

Chen, Y. L. L., H. Y. Chen, I. I. Lin, M. A. Lee, and J. Chang. 2007. "Effects of Cold Eddy on Phytoplankton Production and Assemblages in Luzon Strait Bordering the South China Sea." *Journal of Oceanography* 63 (4): 671–683. doi:10.1007/s10872-007-0059-9.

Chen, Y. Q., and D. L. Tang. 2012. "Eddy-Feature Phytoplankton Bloom Induced by a Tropical Cyclone in the South China Sea." *International Journal of Remote Sensing* 33 (23): 7444–7457. doi:10.1080/01431161.2012.685976.

Clayton, S., S. Dutkiewicz, O. Jahn, and M. J. Follows. 2013. "Dispersal, Eddies, and the Diversity of Marine Phytoplankton." *Limnol Oceanogr Fluids Environment* 3: 182–197. doi:10.1215/21573689-2373515.

Clayton, S., T. Nagai, and M. J. Follows. 2014. "Fine Scale Phytoplankton Community Structure across the Kuroshio Front." *Journal of Plankton Research* 1–14. doi:10.1093/plankt/fbu020.

Dwivedi, R. M., H. U. Solanki, S. R. Nayak, D. Gulati, and V. S. Somvanshi. 2005. "Exploration of Fishery Resources through Integration of Ocean Colour with Sea Surface Temperature: Indian Experience." *Indian Journal of Marine Sciences* 34 (4): 430–440.

He, Q. Y., H. G. Zhan, S. Q. Cai, and Z. M. Li. 2016. "Eddy Effects on Surface Chlorophyll in the Northern South China Sea: Mechanism Investigation and Temporal Variability Analysis." *Deep Sea Research Part I: Oceanographic Research Papers* 112: 25–36. doi:10.1016/j.dsr.2016.03.004.

He, S. Y., D. J. Huang, and D. Y. Zeng. 2016. "Double SST Fronts Observed from MODIS Data in the East China Sea off the Zhejiang–Fujian Coast, China." *Journal of Marine Systems* 154: 93–102. doi:10.1016/j.jmarsys.2015.02.009.

Huang, D. J., T. Zhang, and F. Zhou. 2010. "Sea-Surface Temperature Fronts in the Yellow and East China Seas from TRMM Microwave Imager Data." *Deep Sea Research Part II: Topical Studies in Oceanography* 57 (11): 1017–1024. doi:10.1016/j.dsr2.2010.02.003.

Jing, Z. Y., Y. Q. Qi, B. Fox-Kemper, Y. Du, and S. M. Lian. 2016. "Seasonal Thermal Fronts on the Northern South China Sea Shelf: Satellite Measurements and Three Repeated Field Surveys." *Journal of Geophysical Research: Oceans* 121 (3): 1914–1930. doi:10.1002/2015JC011222.

Jing, Z.-Y., Y.-Q. Qi, Z.-L. Hua, and H. Zhang. 2009. "Numerical Study on the Summer Upwelling System in the Northern Continental Shelf of the South China Sea." *Continental Shelf Research* 29 (2): 467–478. doi:10.1016/j.csr.2008.11.008.

Kahru, M., E. Di Lorenzo, M. Manzano-Sarabia, and B. G. Mitchell. 2012. "Spatial and Temporal Statistics of Sea Surface Temperature and Chlorophyll Fronts in the California Current." *Journal of Plankton Research* 34 (9): 749–760. doi:10.1093/plankt/fbs010.

Lan, K.-W., H. Kawamura, M.-A. Lee, Y. Chang, J.-W. Chan, and C.-H. Liao. 2009. "Summertime Sea Surface Temperature Fronts Associated with Upwelling around the Taiwan Bank." *Continental Shelf Research* 29 (7): 903–910. doi:10.1016/j.csr.2009.01.015.

Landry, M. R., M. D. Ohman, R. Goericke, M. R. Stukel, K. A. Barbeau, R. Bundy, and M. Kahru. 2012. "Pelagic Community Responses to a Deep-Water Front in the California Current Ecosystem: Overview of the A-Front Study." *Journal of Plankton Research* 1–12. doi:10.1093/plankt/fbs025.

Liu, S. M., X. Y. Guo, Q. Chen, J. Zhang, Y. F. Bi, X. Luo, and J. B. Li. 2010. "Nutrient Dynamics in the Winter Thermohaline Frontal Zone of the Northern Shelf Region of the South China Sea." *Journal of Geophysical Research: Oceans* 115: C11. doi:10.1029/2009JC005951.

Mahadevan, A., and A. Tandon. 2006. "An Analysis of Mechanisms for Submesoscale Vertical Motion at Ocean Fronts." *Ocean Modelling* 14 (3): 241–256. doi:10.1016/j.ocemod.2006.05.006.

Mizobata, K., S. I. Saitoh, A. Shiomoto, T. Miyamura, N. Shiga, K. Imai, M. Toratani, Y. Kajiwara, and K. Sasaoka. 2002. "Bering Sea Cyclonic and Anticyclonic Eddies Observed during Summer 2000 and 2001." *Progress in Oceanography* 55 (1): 65–75. doi:10.1016/S0079-6611(02)00070-8.

Parsons, T. R., Y. Maita, and C. M. Lalli. 1984. *A Manual of Chemical and Biological Methods for Seawater Analysis*, 173. Oxford: Pergamon.

Qiu, C. H., D. X. Wang, Z. G. He, and C. Q. Chen. 2012. "Seasonal Variability of Chlorophyll a Fronts in the Luzon Strait Based on Satellite Observations." *Aquatic Ecosystem Health & Management* 15 (1): 46–52. doi:10.1080/14634988.2012.654072.

Rivas, A. L. 2006. "Quantitative Estimation of the Influence of Surface Thermal Fronts over Chlorophyll Concentration at the Patagonian Shelf." *Journal of Marine Systems* 63 (3): 183–190. doi:10.1016/j.jmarsys.2006.07.002.

Saraceno, M., C. Provost, and A. R. Piola. 2005. "On the Relationship between Satellite-Retrieved Surface Temperature Fronts and Chlorophyll a in the Western South Atlantic." *Journal of Geophysical Research: Oceans* 110: C11. doi:10.1029/2004JC002736.

Shi, R., X. Y. Guo, D. X. Wang, L. L. Zeng, and J. Chen. 2015. "Seasonal Variability in Coastal Fronts and Its Influence on Sea Surface Wind in the Northern South China Sea." *Deep Sea Research Part II: Topical Studies in Oceanography* 119: 30–39. doi:10.1016/j.dsr2.2013.12.018.

Shimada, T., F. Sakaida, H. Kawamura, and T. Okumura. 2005. "Application of an Edge Detection Method to Satellite Images for Distinguishing Sea Surface Temperature Fronts Near the Japanese Coast." *Remote Sensing of Environment* 98: 21–34. doi: 10.1016/j.rse.2005.05.018.

Stegmann, P. M., and D. S. Ullman. 2004. "Variability in Chlorophyll and Sea Surface Temperature Fronts in the Long Island Sound Outflow Region from Satellite Observations." *Journal of Geophysical Research: Oceans* 109: C7. doi:10.1029/2003JC001984.

Su, J., and T. Pohlmann. 2009. "Wind and Topography Influence on an Upwelling System at the Eastern Hainan Coast." *Journal of Geophysical Research: Oceans* 114: C6. doi:10.1029/2008JC005018.

Tang, D. L., H. Kawamura, and A. J. Luis. 2002. "Short-Term Variability of Phytoplankton Blooms Associated with a Cold Eddy in the Northwestern Arabian Sea." *Remote Sensing of Environment* 81 (1): 82–89. doi:10.1016/S0034-4257(01)00334-0.

Taylor, A. G., R. Goericke, M. R. Landry, K. E. Selph, D. A. Wick, and M. J. Roadman. 2012. "Sharp Gradients in Phytoplankton Community Structure across a Frontal Zone in the California Current Ecosystem." *Journal of Plankton Research* 34 (9): 778–789. doi:10.1093/plankt/fbs036.

Taylor, J. R., and R. Ferrari. 2011. "Ocean Fronts Trigger High Latitude Phytoplankton Blooms." *Geophysical Research Letters* 38: 23. doi:10.1029/2011GL049312.

Tseng, C.-T., C.-L. Sun, I. M. Belkin, S.-Z. Yeh, C.-L. Kuo, and D.-C. Liu. 2014. "Sea Surface Temperature Fronts Affect Distribution of Pacific Saury (Cololabis Saira) in the Northwestern Pacific Ocean." *Deep Sea Research Part II: Topical Studies in Oceanography* 107: 15–21. doi:10.1016/j.dsr2.2014.06.001.

Vipin, P., K. Sarkar, S. G. Aparna, D. Shankar, V. V. S. S. Sarma, D. G. Gracias, M. S. Krishna, G. Srikanth, R. Mandal, and E. P. R. Rao. 2015. "Evolution and Sub-Surface Characteristics of a Sea-Surface Temperature Filament and Front in the Northeastern Arabian Sea during November–December 2012." *Journal of Marine Systems* 150: 1–11. doi:10.1016/j.jmarsys.2015.05.003.

Wang, D. X., Y. Liu, Y. Q. Qi, and P. Shi. 2001. "Seasonal Variability of Thermal Fronts in the Northern South China Sea from Satellite Data." *Geophysical Research Letters* 28 (20): 3963–3966. doi:10.1029/2001GL013306.

Wang, G. H., J. X. Li, C. Z. Wang, and Y. W. Yan. 2012. "Interactions among the Winter Monsoon, Ocean Eddy and Ocean Thermal Front in the South China Sea." *Journal of Geophysical Research: Oceans* 117: C8. doi:10.1029/2012JC008007.

Yanagi, T., and T. Koike. 1987. "Seasonal Variation in Thermohaline and Tidal Fronts, Seto Inland Sea, Japan." *Continental Shelf Research* 7 (2): 149–160. doi:10.1016/0278-4343(87)90076-8.

Yao, J. L., I. M. Belkin, J. Chen, and D. X. Wang. 2012. "Thermal Fronts of the Southern South China Sea from Satellite and in Situ Data." *International Journal of Remote Sensing* 33 (23): 7458–7468. doi:10.1080/01431161.2012.685985.

Ye, H. J., J. Y. Sheng, D. L. Tang, S. Eko, M. A. Kalhoro, and Y. Sui. 2017. "Storm-Induced Changes in pCO_2 at the Sea Surface over the Northern South China Sea during Typhoon Wutip." *Journal of Geophysical Research: Oceans*. doi:10.1002/2016JC012643.

Ye, H. J., Y. Sui, D. L. Tang, and Y. D. Afanasyev. 2013. "A Subsurface Chlorophyll A Bloom Induced by Typhoon in the South China Sea." *Journal of Marine Systems* 128: 138–145. doi:10.1016/j.jmarsys.2013.04.010.

Yun, K.-S., J. C. Chan, and K.-J. Ha. 2012. "Effects of SST Magnitude and Gradient on Typhoon Tracks around East Asia: Acase Study for Typhoon Maemi (2003)." *Atmospheric Research* 109: 36–51. doi:10.1016/j.atmosres.2012.02.012.

Zeng, X. Z., I. M. Belkin, S. Q. Peng, and Y. N. Li. 2014. "East Hainan Upwelling Fronts Detected by Remote Sensing and Modelled in Summer." *International Journal of Remote Sensing* 35 (11–12): 4441–4451. doi:10.1080/01431161.2014.916443.